Proceedings of the 5th International Conference on Integrity-Reliability-Failure, Porto/Portugal 24-28 July 2016
Editors J.F. Silva Gomes and S.A. Meguid
Publ. INEGI/FEUP (2016)

PAPER REF: 6388

NEW APPROACH TO MODEL THE MECHANICAL BEHAVIOR OF MULTIPLE FRICTION PENDULUM DEVICES

Vincenzo Bianco[1(*)], Giorgio Monti[1], Nicola Pio Belfiore[2]

[1]Department of Structural Engineering and Geotechnics (DISG), Sapienza University of Rome, Rome, Italy
[2]Department of Mechanical and Aerospace Engineering (DIMA), Sapienza University of Rome, Rome, Italy
[(*)]*Email:* vincenzo.bianco@uniroma1.it

ABSTRACT

The adoption of Friction Pendulum Devices (FPD), as a cheaper alternative to the elastomeric bearings, has caught the attention of both academic and technical communities, in the last decades. Even though different versions of such devices can be found on the market and their effectiveness has been extensively proven by means of numerous experimental campaigns carried out worldwide, many aspects concerning their mechanical behaviour still need to be clarified. These aspects concern, among others: 1) sequence of sliding on the several concave surfaces, 2) influence of temperature on the frictional properties of the coupling surfaces, 3) possibility of mechanical stick-slip phenomena, 4) possibility of impact-induced failure of some components, 5) geometric compatibility, and so on. Those aspects are less clear the larger the number of concave surfaces the device is composed of. This paper presents a new way of modelling the mechanical behaviour of the FPDs, by fulfilling 1) geometric compatibility, 2) kinematical compatibility, 3) dynamical equilibrium, and 4) thermo-mechanical coupling.

Keywords: Base isolators, friction pendulum devices, kinematics, dynamic equilibrium.

INTRODUCTION

In recent years base isolation has become an increasingly applied structural design technique for both buildings and bridges located in highly seismic areas. Two basic types of base isolation can be identified (Kelly 1997, Taniwangsa and Kelly 1996): 1) by elastomeric bearings and 2) by a sliding system. According to the former approach, the building or structure is decoupled from the horizontal components of the earthquake ground motion by interposing a layer with low horizontal stiffness between the structure and the foundation. The latter approach works by limiting the transfer of shear across the isolation interface. Many sliding systems have been proposed and some have already been implemented in practice. The Friction Pendulum (FP) system, firstly introduced by Zayas *et al.* (1987), is one of these sliding systems that has already been used for several projects (*e.g.* Mellon and Post 1999), both new and retrofit. It combines a sliding system with a restoring force. In fact it is composed of an articulated slider, whose surface is coated by a special interfacial material with the purpose to provide a suitable friction, sliding on a stainless steel concave surface (Fig. 1a). The concave surface geometrically provides the restoring force as the tangential projection of the applied gravity load. The FP system for seismic isolation has been recently manufactured as devices with multiple independent concave sliding surfaces, in order to provide adaptable behavior (*e.g.* Earthquake Protection Systems, Inc. 2003; Tsai *et al.* 2010). The Double concave Friction Pendulum (DFP) bearing (Constantinou 2004, Fenz and

Constantinou 2006) is an adaptation of the traditional, well-proven single concave friction pendulum that allows for significantly larger displacements, for identical plan dimensions. The DFP bearing consists of two facing stainless steel concave surfaces (Fig. 1b). The upper and lower concave surfaces have radii of curvature R_1 and R_2 that might not be equal. While the coefficients of friction along the two kinematic pairs are μ_1 and μ_2, respectively. An articulated slider separates the two concave surfaces. The articulation is necessary for proper even distribution of pressure on the sliding surfaces and to accommodate differential movements along the top and bottom sliding surfaces when friction is unequal on these two latter. The Triple Friction pendulum bearing (TFP) is an even more advanced version of the original FP (Fig. 1c) that is composed of a) two external concave plates, with radius of curvature and friction coefficient equal to $(R_1; \mu_1)$ and $(R_4; \mu_4)$ respectively, b) two inner sliding plates with radius of curvature and friction coefficient equal to $(R_2; \mu_2)$ and $(R_3; \mu_3)$ respectively, and c) a sliding pad. The external surfaces of both the sliding plates and the sliding pad are coated with a lining material that has to provide the suitable friction coefficient. More recently even friction pendulum bearings presenting more than four sliding surfaces have been proposed (Tsai *et al.* 2010). The more sophisticated versions of the FP, which contemplate the presence of an increasing number of sliding concave surfaces, have the advantage to guarantee: 1) a certain adaptability to the given earthquake, despite being a passive system, as well as 2) a reduced footprint, with the same deformation capacity.

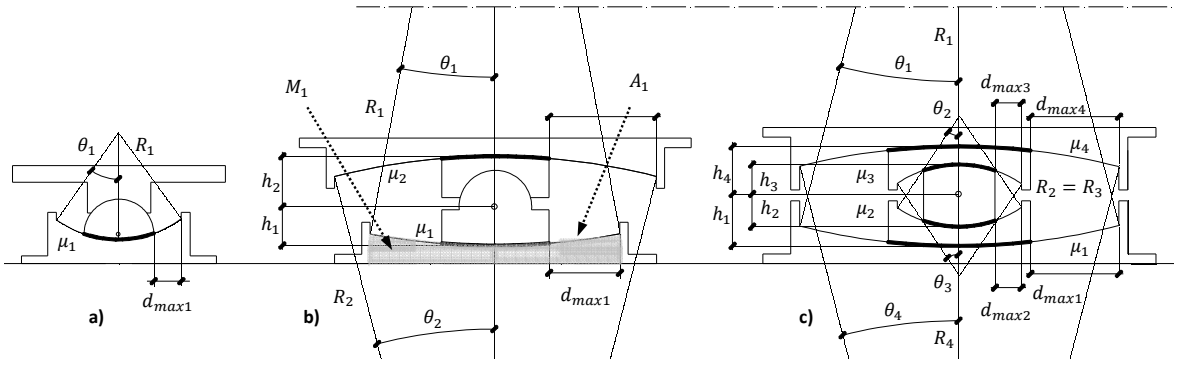

Fig. 1 - Friction pendulum bearings: a) Single Friction Pendulum (SFP), b) Double Friction Pendulum (DFP), c) Triple Friction Pendulum (TFP).

Friction plays a pivotal role in the functioning of the FP devices. However, it is a very complex phenomenon not completely understood yet: it is given by several concomitant physical phenomena whose relative importance varies as function of the involved parameters and contour conditions (*e.g.* Bowden and Tabor 1973; American Society for Metals 1992; Constantinou *et al.* 2007). The most frequently used interface in sliding bearings is made of PTFE or PTFE-like materials in contact with polished stainless steel. For these kind of interfaces, the dynamic coefficient of friction μ mainly depends on (Constantinou *et al.* 1999): a) the sliding velocity, b) pressure, c) temperature and d) time of loading.

Since the introduction of the friction pendulum devices for the seismic protection of structures, a lot of efforts have been made by the scientific community (*e.g.* Mokha *et al.* 1990, Nagarajaiah *et al.* 1991, Fenz and Constantinou 2008) in order to single out the most suitable analytical model of the horizontal force-displacement hysteretic curve characterizing the behavior of such devices. In fact, the hysteretic force-displacement curve needs to be implemented in the standard structural analysis softwares in order to assess the efficacy of the designed intervention to correctly protect the structure against the expected earthquake and in compliance with the code regulations. Even though more refined models of the overall hysteretic curve, each substantially based on the early work by Fenz and Constantinou (2008),

have been recently proposed (*e.g.* Becker and Mahin 2008a,b, Ray *et al.* 2013), they present common drawbacks, among which: 1) equilibrium conditions are fulfilled only in the horizontal direction, completely neglecting the rotational equilibrium, and 2) the influence of thermal effects are completely ignored. In fact, as to this latter aspect, it is well known that, when friction is involved in highly dynamic applications, heat is generated on the contact surfaces as a result of the transformation of mechanical energy into energy of thermal oscillations of molecules during friction. During an earthquake, with peak sliding velocity of the order of $\geq 400\,\mathrm{mm/sec}$, temperature could reach very high values and significantly affect the frictional properties of the PTFE-stainless steel sliding interface.

Moreover, such complex tribological systems are known to be susceptible to 1) the stick-slip and 2) the sprag-slip *phenomena* (*e.g.* Popov 2010). Where: the former consists of the likely alternation of time intervals of sliding to time intervals of no sliding, with consequent re-coupling of the ground shaking and superstructure movement, while the latter consists of vibrations that could be activated in the direction orthogonal to the sliding one.

In this scenario, many questions arise about the actual functioning of these devices. Do they always re-center? Otherwise, under which specific contour conditions, either kinematic (displacements, velocities and accelerations) or tribological (friction) do they re-center? Similarly as what happens with a rolling wheel, must friction have an optimum value, for rolling to take place? In this view, a limit value of asymptotically null friction would allow those devices to work, or would it rather inhibit the triggering of the functioning of the devices? Is it only friction, at each phase of the device deformation, that dictates the triggering, rather than the inhibition, of sliding along the various concave surfaces? How does rotational equilibrium affect this aspect? Does the over-structure actually horizontally translates only, without any rotation, during an earthquake lacking the vertical component? Otherwise, under which specific conditions the over-structure does not undergo any rotation? Would it be necessary to outfit the isolation system with supplemental devices meant to suppress any possibility of rotation? Does the building actually move upward, as a response of the horizontal two dimensional earthquake? Or rather, as function of the soil deformability, it may move downwards, in order to accommodate vertical deformations? Does a complex soil-structure interaction take place during an earthquake?

It is evident that the topic is complex and needs to be faced from a multidisciplinary standpoint, involving also both mechanical and tribological engineering expertize (*e.g.* Scotto Lavina 1990, Belfiore *et al.* 2000).

With the aim to contribute to a better understanding of the mechanical behavior of the multiple FPs, thus attempting to answer the questions above, this work presents a new approach to model the thermo-mechanical behavior of such devices. It assumes, as a first approximation, that all the components the device is made of can be modelled as rigid bodies, thus neglecting, for the time being, any deformation. This modelling approach is aimed at fulfilling: 1) geometrical compatibility, 2) kinematic compatibility, 3) dynamic equilibrium, both translational and rotational, and 4) thermo-mechanical coupling.

INSPIRING PHYSICAL OBSERVATION

Suppose to have a kind of flat double friction bearing (Fig. 2), composed of a) two rigid horizontal steel plates, and b) a rigid steel cylinder placed in between. Imagine that this device is loaded by a vertical force N and that friction at the two interfaces is governed by the Coulomb constitutive law (Fig. 2b), with a rigid-perfectly-plastic dependence of the friction

force on the relative displacement $F(u)$, and threshold value $F_\mu = \mu \cdot N$. Imagine also that the friction coefficient μ at those interfaces, has the same value. If we impose a displacement on the lower plate, due to the rigid-plastic constitutive law of interfacial friction, we would immediately have, even for infinitesimally small values of imposed displacement, the mobilization of the friction threshold F_μ at each interface. Those two horizontal forces, equal in magnitude and opposite in direction, do generate a couple, to which corresponds a moment $M_S = F_\mu \cdot H$ that, in the initial configuration, is not balanced by any other couple. That moment would tend to overturn the pad by making it rotate around one of the corners. In such tentative rotation, the points of application of the vertical force N would migrate to the pad corners still in contact with the relevant horizontal plates. In this way, even the vertical force would give rise to a couple $M_R = N \cdot d$, opposed to the overturning one and larger in absolute value, that would make the pad undergo both a rigid body rotation around its centroid G and a simultaneous vertical translation. During such movement of the pad, the diagonally opposed corners, loaded by N, would also undergo sliding, up to the new, restored equilibrium configuration (Fig. 2e). It is the vertical weight force N that restores the geometric compatibility at each time step.

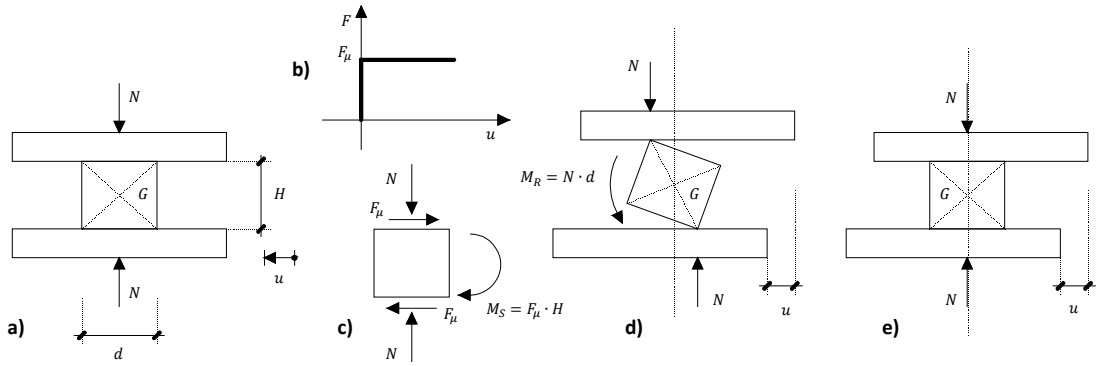

Fig. 2 - Case of a flat double friction bearing: a) undeformed initial configuration, b) friction's Coulomb constitutive law, c) pad free body diagram, d) intermediate deformed configuration, and e) final configuration of the whole device.

GEOMETRIC COMPATIBILITY

When it comes to multiple friction pendulum bearings, namely with concave spherical surfaces, the most advanced device currently available on the market is the Triple Friction Pendulum (TFP). It is composed of (Fig. 3): a) two external concave-surface-topped plates, both with radius $R = R_1 = R_4$, b) two internal sliding plates, which are two straight cylinders whose bases, one convex and another concave, are two spherical caps belonging to two spherical surfaces with different radii, $R_1 \neq R_2$ and $R_3 \neq R_4$ respectively, and c) an internal sliding pad, which is a straight cylinder with both bases composed of convex spherical caps belonging to surfaces with the same radius $R_2 = R_3$. The two external faces of the two larger plates are horizontal. The four sliding interfaces are composed by the superimposition, in pairs, of eight spherical caps, one constituted of plain stainless steel and the other coated by a particular liner, that is generally PTFE or the like.

The considerations herein presented are based on the following assumptions: the various parts constituting the *friction pendula* are considered as rigid bodies, thus neglecting, at least for the time being, any possible deformation. In this way, geometrical compatibility is fulfilled each

time the two spherical caps constituting the two mating surfaces of a given interface are perfectly superimposed to each other.

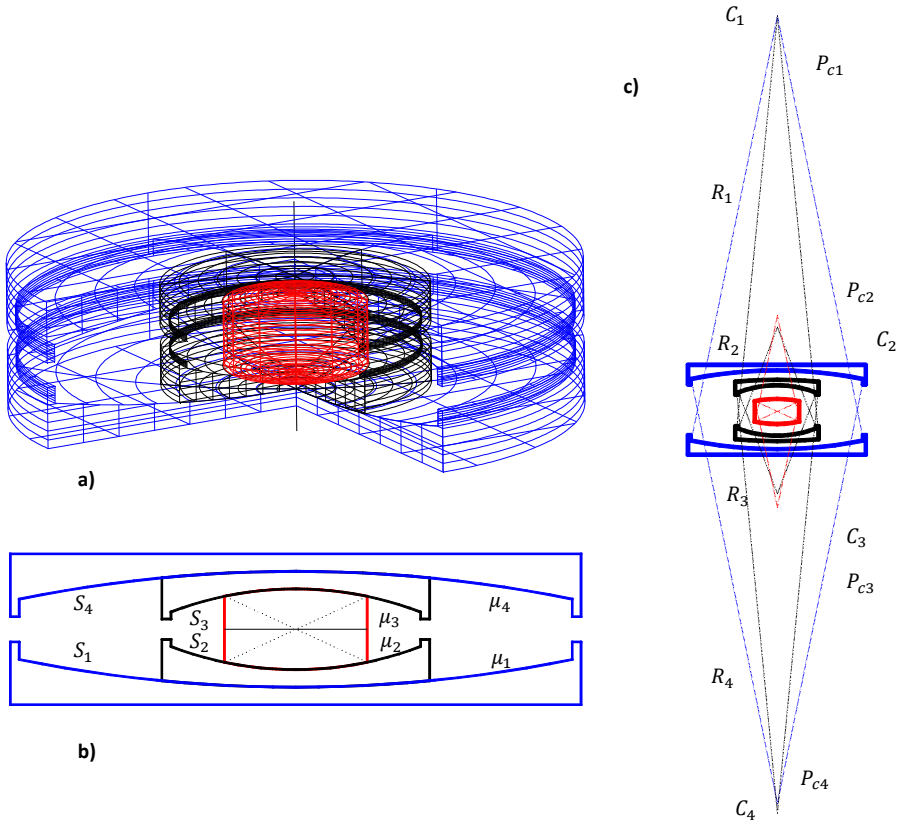

Fig. 3 - Triple Friction Pendulum device: a) axonometric section, b) plan section, and c) exploded plan section.

The first and most important constraint is represented by the fact that the two outermost horizontal surfaces, lower and higher, can undergo a rigid body motion remaining horizontal, which means that they can only translate remaining parallel to themselves. This is due to the fact that, at the extrados of the so called isolation plane, the various isolators are connected by a rigid diaphragm (*e.g.* Italian Technical Regulations 2008) while, at the intrados, to the presence of the ground. In order for that condition to be fulfilled, it is necessary that either the two internal surfaces (S_2 and S_3) or the two external ones (S_1 and S_4) undergo sliding simultaneously while it is not preferable to allow mixed sliding, *e.g.* S_2 and either S_1 or S_4, since controlling the evolution of displacements along each concave surface would become extremely difficult. For this reason, the friction coefficient should be the same along the two surfaces of each of those two sliding pairs, *i.e.* $\mu_2 = \mu_3$ and $\mu_1 = \mu_4$.

It is preferable to start by analyzing the behavior of a double friction pendulum, composed of the internal pad and only two external plates, in a radial plane, which means in case of uni-directional imposed horizontal displacement (Fig. 4). At a generic time step t_n, the internal deformation undergone, as function of the imposed displacement $\Delta u_g(t_n)$, by the several members constituting the device, can be decomposed into two subsequent phases. When starting from the equilibrium condition (Fig. 4a-d), in the first phase, which means during the first part Δt_1 of the time increment Δt, the pad, due to the imposed displacement $\Delta u_g(t_1)$, rigidly rotates around one of the lowermost corners (A) and such rotation also yields a certain vertical displacement of the upper plate. During the second phase Δt_2 of the current time

increment Δt, the pad undergoes a rigid rotation around its centroid (E) with this latter simultaneously rigidly translating along the straight line connecting the centers of the two spherical surfaces $\overline{C_1C_2}$. This latter direction, resulting from the end of the previous sub-interval Δt_1, is inclined, with respect to the vertical direction, of an angle $\theta(t_1)$ that is the geometrical variable accounting for the final configuration assumed by the entire device (Fig. 4d). The same two-step deformation can be recognized if, at a generic time step t_n, the ground imposes a reversed displacement, and starting from a generic deformed configuration (Fig. 4e-h). The only difference, in case of reversal, is that initial rigid rotation (Δt_1) involves the other diagonal of the pad (*i.e.* $\overline{DB}$ instead of $\overline{AC}$). During the second phase, sliding occurs along the corners of the involved diagonal of the pad, and friction is mobilized therein.

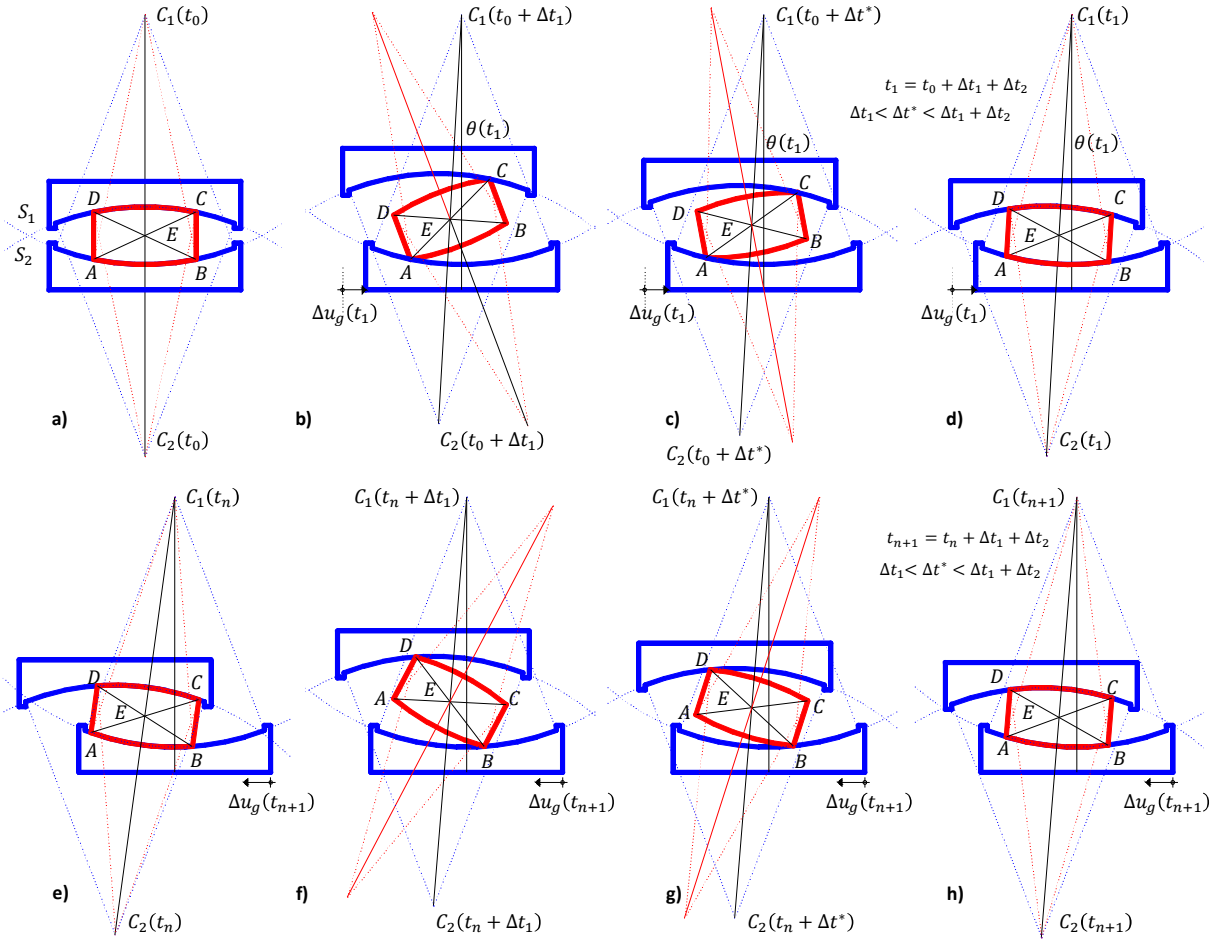

Fig. 4 - Case of a Double Friction Pendulum device subjected to an horizontal ground displacement contained in a radial plane: a-d) rightward ground movement starting from a rest position, and e-h) leftward movement starting from a maximum deformation.

The same two-step deformation at a generic instant t_n can be singled out when a more general situation is considered, in which we assume that 1) the pad is already dislocated ($\theta(t_n), \varphi(t_n)$) from the equilibrium configuration, and 2) the ground-imposed displacement $\Delta u_g(t_n)$ is generically oriented with respect to an external and fixed reference system $oxyz$ (Fig. 5). Even though already dislocated at the start (t_n) of the current incremental time step, the pad must have restored, according to the two-step deformation above, a geometrically compatible configuration (Fig. 5a). Such displaced configuration, uniquely identified by the two spherical coordinates $\theta(t_n)$ and $\varphi(t_n)$, that are the polar and azimuthal angle respectively

(Fig. 5), is thus characterized by the fact that the pad axis $\overline{P_{c1}P_{c2}}(t_n)$ is superimposed on the segment $\overline{C_1C_2}(t_n)$ connecting the two centers of the external spherical surfaces.

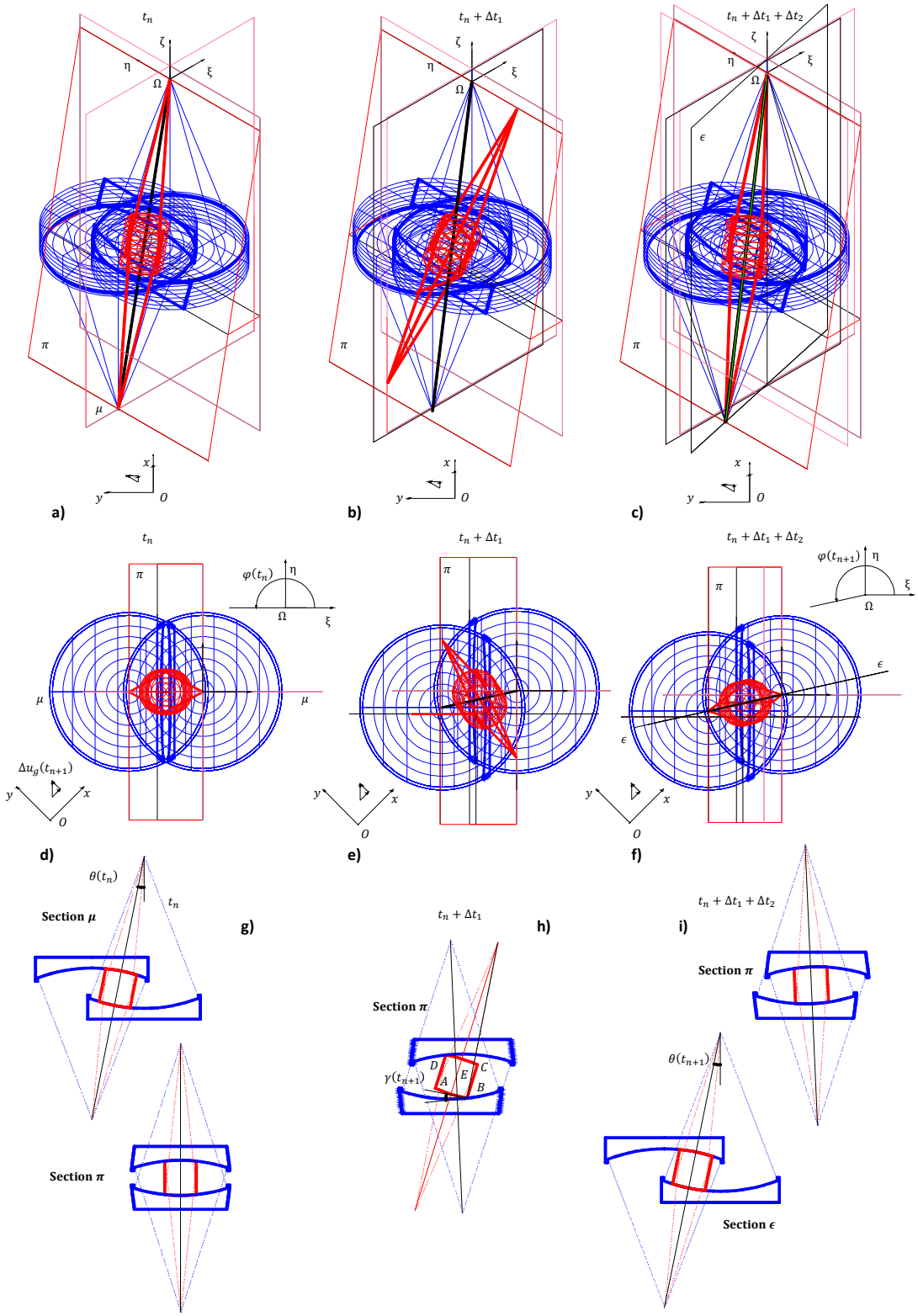

Fig. 5 - Case of a Double Friction Pendulum device subjected to an horizontal ground displacement generically oriented with the pad already dislocated from the initial equilibrium configuration: a-c) 3D axonometric representation of the two-step deformation, d-f) corresponding planar views, and g-i) planar cross-sections.

Whatever the orientation of the imposed displacement $\Delta u_g(t_n)$ in $oxyz$, it is always possible to single out a plane π passing through that displacement orientation and the two centers of the spherical surfaces (one is sufficient indeed, provided that the geometrical compatibility was fulfilled). The geometrically compatible two-step deformation takes place in the plane π that, since passing through the spheres' centers, sections these latter along two circles with maximum radius, *i.e.* $R_\pi = R_1 = R_2$. The two-step deformation is again composed of 1) a rigid body rotation along one of the corners of the pad (which means a point, in 3D), contained in the plane π, and 2) a subsequent simultaneous rigid rotation and translation of the pad, always contained in π, that restores compatibility, as can be gathered from the planar cross sections plotted in Fig. 5. During the second phase (Δt_2), sliding occurs, simultaneously to the rigid roto-translation, along the corners of the pad. When geometrical compatibility is restored, spherical coordinates assume updated values $\theta(t_{n+1}), \varphi(t_{n+1})$ (Fig. 5f and i).

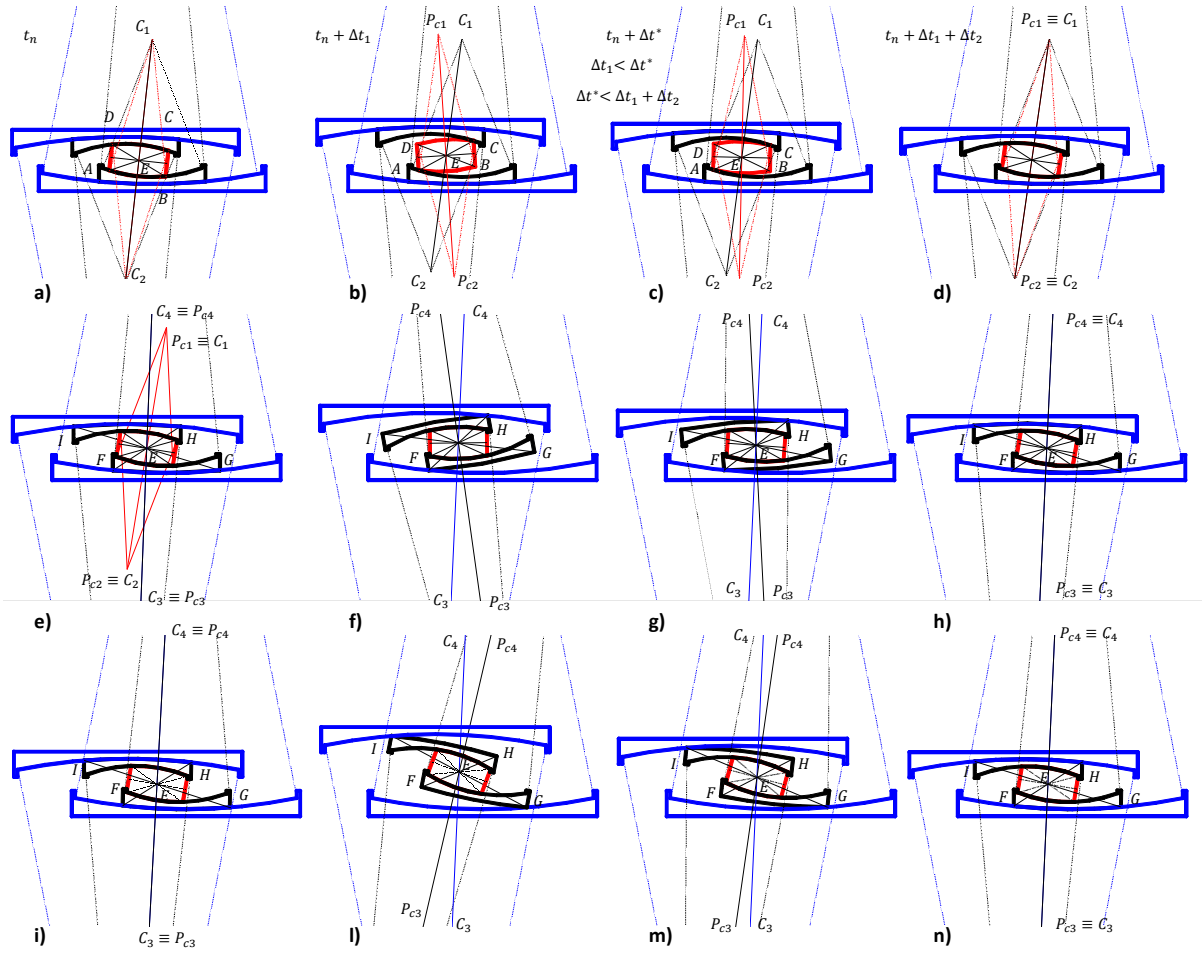

Fig. 6 - Case of a Triple Friction Pendulum device subjected to a uni-directional ground displacement with the pad already dislocated from the initial equilibrium configuration: (a-d) case of sliding occurring only along the pad external surfaces, (e-h) case of sliding occurring only along the external surfaces of the internal plates, with the pad frozen in its maximum deformation, and (i-n) case of reversal with the pad frozen in its maximum deformation.

When a complete triple friction pendulum device is taken into consideration, the same principles, though further complicated by the larger number of geometrical variables involved, apply (Figs. 6 and 7). It is convenient, for the time being, to analyze just the planar behavior of the TFP. If sliding is expected to occur only along the pad external surfaces

(Fig. 6a-d), the situation is substantially identical to what has already been discussed about the case of the DFP.

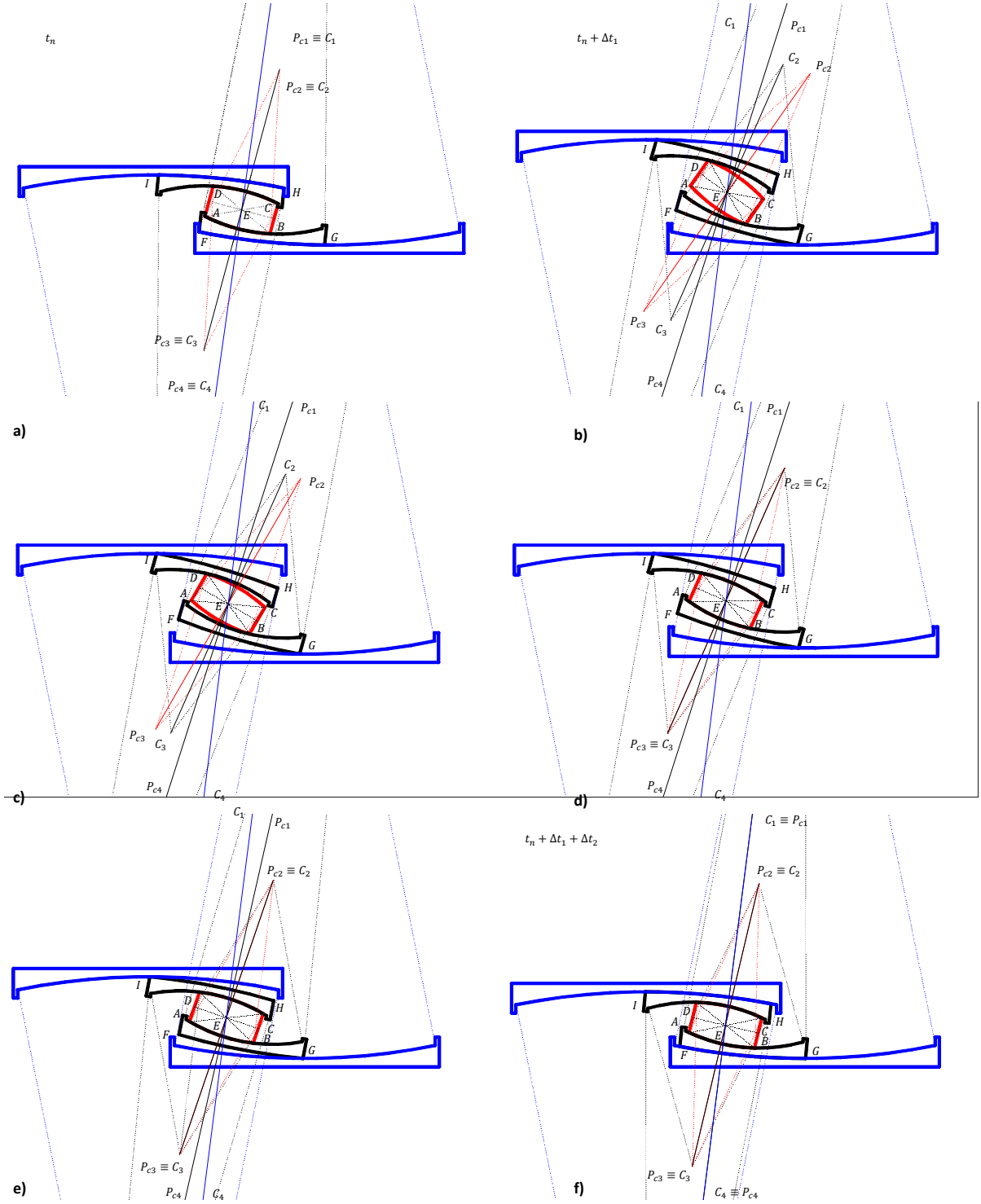

Fig. 7 - Case of a Triple Friction Pendulum device subjected to a uni-directional horizontal ground displacement during reversal: (a,b) first, (c,d) second, and (e,f) third phase, necessary to restore geometric compatibility.

If it is assumed, as it would be preferable in order to more easily control the possible deformation undergone by the whole device during an earthquake, that sliding occurs on the external surfaces only, after the inner ones have reached their capacity, again, the situation is

substantially identical to what has already been discussed for the DFP, except that the pad now has a dissymmetric shape (Fig. 6e-h) and the first phase rigid rotation concerns either the shorter or the longer diagonal, depending on if the motion is forward oriented (Fig. 6e-h) or under reversal (Fig. 6 i-n).

In case it is admitted and allowed that, on reversal, both pairs of sliding surfaces ($\mathcal{S}_2, \mathcal{S}_3$ and $\mathcal{S}_1, \mathcal{S}_4$) can simultaneous slide, even if, as stated above, this would mean that, when the device passes again from the position of null displacement $u_g(t_n) = 0$, geometrical compatibility might not be fulfilled, the phases the whole system needs to undergo in order to settle in the new compatible configuration for the current value of the imposed displacement, are three. A first phase (Δt_1) in which, given the new value of imposed displacement increment $\Delta u_g(t_{n+1})$, the pad rigidly rotates around one of its corners (*e.g.* B in Fig. 7b) and the pair of internal plates rigidly rotates around one of their corners (*e.g.* G in Fig. 7b). Then a second phase (Δt_2) in which the pad undergoes a rigid roto-translation, with its instantaneous rotational center (E in Fig. 7c,d) moving along the line passing through the two mating concave surfaces' centers $\overline{C_2C_3}$ up to full restoration of geometric compatibility with segment $\overline{P_{c2}P_{c3}}$ perfectly superimposed to $\overline{C_2C_3}(t_n + \Delta t_1)$ (Fig. 7d). During this phase some work is done by friction for the sliding along contact vertices D and B. Then a third phase (Δt_3) in which the two internal plates also restore a geometrically compatible configuration by undergoing a rigid roto-translation with the instantaneous rotational center E moving along the straight line passing through the segment $\overline{C_1C_4}(t_n + \Delta t_2)$, up to the instant ($t_{n+1} = t_n + \sum_{i=1}^{3} \Delta t_i$) in which segment $\overline{P_{c1}P_{c4}}$ has fully superimposed to $\overline{C_1C_4}$. Also during this last phase sliding simultaneously occurs along the vertices I and G and some work is done there by friction. If such simultaneous sliding of surfaces is contemplated, the study of the kinematic compatibility in a three dimensional representation would be much more complex, so that further research would be necessary.

MECHANICAL MODEL

The analysis of the geometric compatibility of the friction pendulum devices described in the previous section suggests, in a consequential manner, the way in which it is possible to model the mechanical behavior of such devices in the three dimensional space. For the reasons already explained in the previous section, in the present work attention is focused on the dynamical behavior of a DFP subjected to a ground shaking, leaving the study of complete TFP to further future developments. Moreover, the study is herein limited to the case of unidirectional seismic attack. The dynamical behavior of a DFP at the instant t_n can therefore be limited to what happens in the generic plane π, singled out by 1) current position of the pad ($\theta(t_n), \varphi(t_n)$), and 2) direction, in the reference system $oxyz$, of the current horizontal displacement $\Delta u_g(t_{n+1})$ imposed by the ground shaking, excluding any vertical earthquake, for the time being. Both phases at the current time step can be modelled by an articulated system of rigid bodies, different for each phase (Fig. 8). Even though the rigid bodies are expected to actually undergo some deformations, for the time being they are herein assumed to behave as perfectly rigid bodies. These latter form an open kinematic chain for both phases of motion.

During the first phase (Δt_1), the lower plate (Rigid Body 1) is assumed to move horizontally along a prismatic guide, without friction, and the motion is the one imposed by the earthquake and characterized by given displacement $x_g(t_{n+1})$, velocity $\dot{x}_g(t_{n+1})$, and acceleration

$\ddot{x}_g(t_{n+1})$. The pad (Rigid Body 2) is kinematically constrained to both lower and upper plate (RB 3,4) by two revolute joints in which the constraint force tangent to the concave surface is blocked to the maximum allowable Coulomb friction force. The upper sliding plate (RB 3) carries the weight of the over-structure that is herein assumed as a mass, rigidly connected to the plate by a massless rigid rod, and concentrated in rigid body 4. Substantially, rigid bodies 3 and 4 are assumed to form a single rigid body assemblage. Due to the motion imposed on rigid body 1, rigid body 2 undergoes a rigid rotation β_1 around one of its corners (point A in Fig. 8a) characterized by angular velocity and acceleration $\dot{\beta}_1$, $\ddot{\beta}_1$. As a consequence of that (unknown) rotation, the assemblage of rigid bodies 3 and 4 undergoes a rigid planar translation, along axes x and z of the inertial reference system $oxyz$, maintaining contact with the pad in the pin-joint in point C of the pad. Note that the position assumed by the plates at the end of this first phase already singles out the final updated value of the inclination of the pad with respect to both the sliding plates $\theta(t_{n+1})$.

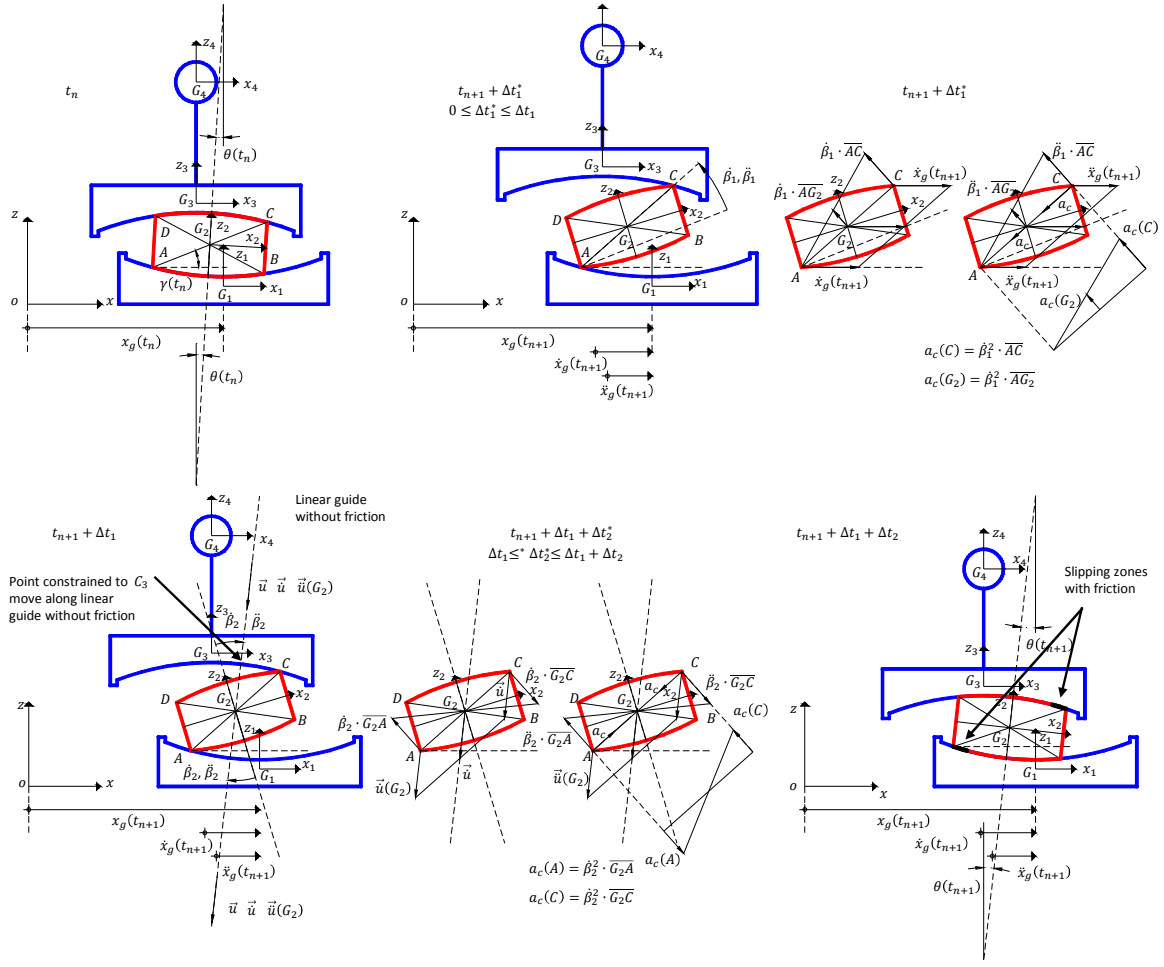

Fig. 8 - Mechanical models, constituted of Articulated System of Rigid Bodies (ASRB), to simulate the two-phases behavior of the DFP at a given time step: a) first phase ASRB and b) second phase ASRB.

The second phase is modelled by the same assemblage of rigid bodies above, kinematically constrained between one another in a different way (Fig. 8b). Rigid body 1 is blocked in its final position corresponding to the current time step t_{n+1}. Rigid body 2 undergoes a rigid roto-translation with its centroid G_2 translating along the straight line connecting the two centers of curvature of the two plates, along a linear prismatic guide without friction and contemporarily counter-rotates around its centroid with angular velocity and acceleration

$\dot{\beta}_2$, $\ddot{\beta}_2$. Along the vertices of the diagonal involved ($\overline{AC}$ in Fig. 8), the pad is now constrained to the two plates (rigid bodies 1 and 3) by two circular guides with Coulomb friction so that, during this phase, slipping takes place with consequent yielding of heat (Fig. 8b). While kinematic quantities $\vec{\ddot{u}}(G_2)$ and $\dot{\beta}_2$, which are the linear and angular accelerations characterizing the pad rigid roto-translation, are unknown since depend on the dynamical characteristics of the system, the values of displacement $\vec{u}(G_2)$ and rotation β_2 are known since they are the quantities necessary to restore the geometrical compatibility by closing both kinematic couples implying that the pad axis superimposes to the straight line connecting the concave plates centers (compare previous sections). The assemblage of rigid bodies 3 and 4 translate with point C_3 moving (Fig. 8b), without friction, along the straight line connecting the concave surfaces' centers $\overline{C_1C_2}(t_n + \Delta t_1)$.

KINEMATIC COMPATIBILITY

A kinematic analysis, meant to study motion without considering the forces that produce it, is necessary. During the first phase, the velocity of point C, in which a revolute joint is placed, is given by (*e.g.* Scotto Lavina 1990, Belfiore *et al.* 2000):

$$\overrightarrow{v_C} = \overrightarrow{v_A} - \dot{\beta}_1 \cdot \overrightarrow{e_2} \times \overrightarrow{AC} = \dot{x}_g \cdot \overrightarrow{e_1} - \dot{\beta}_1 \cdot \overrightarrow{e_2} \times \overrightarrow{AC} \quad (1)$$

where $\overrightarrow{e_2}$ is the unit vector of axis y of the Inertial system $oxyz$ whose positive direction is towards the paper. While the acceleration is given by:

$$\overrightarrow{a_C} = \overrightarrow{a_A} + \overrightarrow{a_c}(C) - \ddot{\beta}_1 \cdot \overrightarrow{e_2} \times \overrightarrow{AC} = \ddot{x}_g \cdot \overrightarrow{e_1} + \dot{\beta}_1^2 \cdot \overrightarrow{G_2A} - \ddot{\beta}_1 \cdot \overrightarrow{e_2} \times \overrightarrow{AC} \quad (2)$$

During the second phase, the velocity of point C, belonging to rigid body 2 (pad) is given by:

$$\overrightarrow{v_C} = \vec{\ddot{u}}(G_2) + \dot{\beta}_2 \cdot \overrightarrow{e_2} \times \overrightarrow{G_2C} \quad (3)$$

while the velocity with which the rigid bodies 3 and 4 translate along the linear prismatic guide without friction, along the straight line connecting the position occupied by the two curvature centers at the end of step one, is given by the velocity of point C_3 (Fig. 8b):

$$\overrightarrow{v_{C_3}} = \vec{\ddot{u}}(G_2) \quad (4)$$

The acceleration of point C, belonging to rigid body 2, is given by (Fig. 8b):

$$\overrightarrow{a_C} = \vec{\ddot{u}}(G_2) + \overrightarrow{a_c}(C) + \ddot{\beta}_2 \cdot \overrightarrow{e_2} \times \overrightarrow{G_2C} = \vec{\ddot{u}}(G_2) + \dot{\beta}_2^2 \cdot \overrightarrow{G_2C} + \ddot{\beta}_2 \cdot \overrightarrow{e_2} \times \overrightarrow{G_2C} \quad (5)$$

and the acceleration of point C_3, is given by:

$$\overrightarrow{a_{C_3}} = \vec{\ddot{u}}(G_2) \quad (6)$$

DYNAMICAL EQUILIBRIUM

Both mechanical models adopted to study the two phases of the planar motion of the DFP described in previous section are open kinematic chains (Shabana 2001). And each of them is characterized by one degree of freedom.

In fact, for the first phase, we have 3 rigid bodies, each characterized by 3 kinematic unknowns, for a total of $n = 3 \times 3 = 9$. The number of kinematic constraints is equal to $n_c = 7$ that are given by: a) vertical translation and rotation (2) of the RB1, b) two internal revolute joints ($2 \times 2 = 4$), and c) rotation (1) of the assemblage of RB3 and RB4. The

translational horizontal degree of freedom of the lowermost sliding plate (RB1) is kinematically controlled by the earthquake, while the rotational degree of freedom of the pad is not known *a priori* so that a force analysis is required and the system equations of motion must be formulated to obtain a number of equations equal to the number of unknown variables.

For the second phase, we have $n = 3 \times 3 = 9$ kinematic unknowns. The number of kinematic constraints is equal to $n_c = 8$ that are given by: a) 3 for the lowermost plate that is assumed fixed, b) 1 for the pad, since its centroid G_2 cannot move orthogonally to the straight line (prismatic frictionless guide) passing through the concave surfaces centers $\overline{C_1C_2}(t_n + \Delta t_1)$, c) 2 for the uppermost sliding plate assembled with the over-structure (Rb3+RB4), since they can only translate with the contact point at the end of phase 1 (*i.e.* point C_3 in Fig. 8b) moving along the straight line above, thus neither rotating nor translating orthogonally to that line, and d) 2 are given by the internal constraints constituted by the circular frictional prismatic guides, between the kinematic couples RB1-RB2 and RB2-RB3+RB4, since they do not allow mutual displacement at the contact point, along the relevant radius of curvature. The independent kinematic unknown is $\ddot{\beta}_2$ while the translational acceleration $\ddot{u}(G_2)$ can be expressed as function of $\ddot{\beta}_2$.

The first kinematic chain is both *kinematically* and *dynamically driven* (Shabana 2001) since one degree of freedom, that is the horizontal translation of the lowermost plate, is imposed by the ground movement and another, that is the rotation around one of the pad's corners, is governed by the forces involved, either inertia and external. On the other hand, the second kinematic chain is *dynamically driven*, since for the unknown, a force analysis is required. For both models, a relevant minimum number of differential equations can be written, in the ambit of the Embedding Technique (Shabana 2001), by making a suitable cut in one of the joints among the involved rigid bodies, and formulating the dynamic conditions of the resulting subsystem. The number of these obtained equations, which do not contain the joint reaction forces, is equal to the number of degrees of freedom of the system. Once the minimum number of differential equations are solved, the joint reaction forces can be obtained by the equations of motion obtained by a free-body analysis.

Proceeding in this way, for both phases' kinematic chain, making the cut in correspondence of the revolute joint in point A, the following equilibrium equation, applying the D'Alambert principle, is obtained:

$$\vec{K}_A = \vec{K}_{G_2} + \overrightarrow{AG_2} \times \frac{d}{dt}\vec{Q}_2 + \overrightarrow{AG_3} \times \frac{d}{dt}\vec{Q}_3 + \overrightarrow{AG_4} \times \frac{d}{dt}\vec{Q}_4 = \vec{M}_A = \sum_{i=2}^{4} \overrightarrow{AG_i} \times \vec{P}_i \qquad (7)$$

in which: $\vec{K}_A$ is the moment of the inertia forces with respect to point A, $\vec{K}_{G_2}$ is the moment of inertia of RB2 with respect to its centroid, $\vec{Q}_i$ is the momentum of the i-th RB, $\vec{M}_A$ is the moment of the external forces with respect to point A, and $\vec{P}_i$ is the self-weight force of the i-th RB. For each phase, Eq. (7) has to be specialized by substituting, in the expression of the i-th RB time-derivative of the momentum, the kinematically compatible expressions for the accelerations, as obtained in the previous section.

THERMO-MECHANICAL COUPLING

During the second phase, slipping occurs along the two concave surfaces (Fig. 8b) and heat is developed therein. It is possible both 1) to keep track of the temperature change of the plates

and 2) to evaluate the change of the frictional threshold as function of the surface temperature. Thermo-mechanical coupling is obtained by defining a suitable law of variation of the frictional coefficient, as function of the temperature, as follows:

$$F_{\mu i}(t) = \mu_i[T_i(t)] \cdot N_i \quad (8)$$

where: $F_{\mu i}(t)$, μ_i, $T_i(t)$, N_i are a) the friction strength, b) the temperature dependent friction coefficient, c) the temperature, and d) the internal force orthogonal to the *i*-th concave surface.

At each time step, the increment of Temperature, yielded by the friction-induced heat, can be evaluated by the following thermal equilibrium equation:

$$c_i \cdot \dot{T}_i = f_i \cdot \dot{u}_i - \dot{Q}_i \quad (9)$$

where: $\dot{T}_i$ is the rate of change of temperature ($temperature/time$), c_i is the heat capacity ($energy/temperature$) of the i-th surface, given by the product of the steel specific heat c_s times the mass M_i of the concave surface involved in the heat exchange, and $\dot{Q}_i$ is the rate of heat exchanged with the surrounding environment ($energy/time$). For the sake of simplicity, M_i can be assumed coincident with the whole mass of the relevant steel plate (Fig. 1).

Moreover, the following assumptions may be made: 1) heat is generated by friction at each of the sliding interfaces, 2) heat conduction is assumed unidirectional, perpendicular to each concave surface, 3) heat loss due to radiation is assumed negligible, 4) bearing material (*PTFE* or the like) is assumed as a perfect thermal insulator so that heat generated at the sliding interface just flows towards each concave surface (in fact the thermal diffusivity of steel is $\sim 20.0\, W/m \cdot °C$ that is much larger than the one of PTFE $\sim 0.24\, W/m \cdot °C$ at $20°C$ temperature).

The rate of heat exchange $\dot{Q}_i(\mathrm{T}, \mathrm{t})$ by the i-th surface with the surrounding environment can be modelled by the Newton's law of cooling that is usually adopted to describe convective heat exchanges, that is:

$$\dot{Q}_i(T, t) = H_i \cdot (T_i - T_{air}) \quad (10)$$

where: H_i is the i-th concave surface heat transfer coefficient ($heat/temperature \cdot time$), given by the product of the steel convectional heat exchange coefficient h_s times the area A_i of the portion of the concave surface effectively exchanging heat with the surrounding air whose temperature is T_{air}.

CONCLUSION

The so called Friction Pendulum Devices are seismic bearings that have been recently capturing the attention of both Academic and Technical communities as a suitable and relatively cheaper alternative to the elastomeric bearings. However, even though their effectiveness has been proven by numerous experimental campaigns carried out worldwide, they are complex tribological systems, composed of different kinematic couples, whose mechanical behavior is far from trivial. Many aspects still need to be clarified and it seems necessary to involve also mechanical and tribological expertize. Among those aspects, there's the need to clarify phenomena such as *stick-slip* and *sprag-slip*, which have also been observed experimentally.

Moreover, most of the theoretical works available in the literature, aimed at reproducing the force-displacement hysteretic curve, have completely neglected the rotational and vertical translation of such devices during an horizontal ground motion. And they also seem to have not paid due attention to the geometrical compatibility.

In the present work, a new approach to model the mechanical behavior of such devices was proposed. It started from analyzing the likely geometrical compatibility of such devices during their functioning and ended up proposing a two-step deformation that restores geometric compatibility at each time step and also accounts for the possibility of stick-slip to occur. The main features of such approach, which is based on 1) geometrical compatibility, 2) kinematical compatibility, 3) dynamic equilibrium, and 4) thermo-mechanical coupling, were delineated.

For the time being, only the formal aspects of this approach were herein presented, and limited to the planar deformation of a DFP. As further developments, such approach will be extended to tridimensional behavior of both DFP and TFP. This will be done paying due attention to tribological issues of a) wear, b) thermal-induced effects, and c) selection of the most suitable liner. Also questions related to the impact between the several components will be addressed.

REFERENCES

[1]-American Society for Metals. Friction, Lubrication, and Wear Technology. ASM Handbook, Vol. 18, Metals Park, Ohio, 1992.

[2]-Becker, T.C., Mahin, S.A. Experimental and analytical study of the bi-directional behavior of the triple friction pendulum isolator. Earthquake Engineering and Structural Dynamics, 2012a, 41(3), p. 355-373.

[3]-Becker, T.C., Mahin, S.A. Correct treatment of rotation of sliding surfaces in a kinematic model of the triple friction pendulum bearing. Earthquake Engineering and Structural Dynamics, 2012b, 42(2), p. 311-317.

[4]-Belfiore, N.P., Di Benedetto, A., Pennestrì, E. Fondamenti di meccanica applicata alle macchine. Casa Editrice Ambrosiana, 2000.

[5]-Bowden, F.P., Tabor, D. Friction; an Introduction to Tribology. Heinemann, UK, 1973.

[6]-Constantinou, M.C., Tsopelas, P., Kasalanati, A., Wolff, E.D. Property modification factors for seismic isolation bearings. Technical Report MCEER-99-0012, Multidisciplinary Center for Earthquake Engineering Research, State University of New York at Buffalo, Buffalo, NY, 1999.

[7]-Constantinou, M.C. Friction Pendulum double concave bearing. NEES Report, available at: http://nees.buffatlo.edu/docs/dec304/FP-DC%20Report-DEMO.pdf, 2004.

[8]-Constantinou, M.C., Whittaker, A.S., Kalpakidis, Y., Fenz, D.M., and Warn, G.P. Performance of Seismic Isolation Hardware under Service and Seismic Loading. Technical Report MCEER-07-0012, Multidisciplinary Center for Earthquake Engineering Research, State University of New York at Buffalo, Buffalo, NY, August 2007.

[9]-Earthquake Protection Systems (EPS), Inc. Technical characteristics of friction pendulum bearings. Technical Report, Vallejo, California, 2003.

[10]-Fenz, D.M., Constantinou, M.C. Behaviour of the double concave Friction Pendulum bearing. Earthquake Engineering and Structural Dynamics, 2006, 35, p. 1403-1424.

[11]-Fenz, D.M., Constantinou, M.C. Spherical sliding isolation bearings with adaptive behavior: Experimental verification. Earthquake Engineering and Structural Dynamics, 2008, 37, p. 185-205.

[12]-Italian Technical Regulations, Norme Tecniche per le Costruzioni, NTC2008, Italy.

[13]-Kelly, James. M. Earthquake-Resistant Design with Rubber". 2nd ed. Berlin and New York, 1997, Springer-Verlag.

[14]-Mellon, D., Post, T. Caltrans Bridge Research and Applications of New Technologies. In: Proceedings of U.S.-Italy Workshop on Seismic Protective Systems for bridges, Multidisciplinary Center for Earthquake Engineering Research, Buffalo, NY, 1999.

[15]-Mokha, A., Constantinou, M.C., Reinhorn, A.M. Experimental study and analytical prediction of earthquake response of sliding isolation system with spherical surface. Technical Report NCEER-90-0020, National Center for Earthquake Engineering Research, University at Buffalo, SUNY, Buffalo, 1990.

[16]-Nagarajaiah, S., Reinhorn, A.M., Constantinou, M.C. Nonlinear dynamic analysis of 3D base isolated structures. ASCE Journal of Structural Engineering 1991, 117(7), p. 2035-2054.

[17]-Popov, V. Contact Mechanics and friction – physical principles and applications. Springer, Berlin, 2010.

[18]-Ray, T., Sarlis, A.A., Reinhorn, A.M., Constantinou, M.C. Hysteretic models for sliding bearings with varying frictional force. Earthquake Engineering and Structural Dynamics, 2013, 42(15), p. 2341-2360.

[19]-Scotto Lavina, G. Riassunto delle Lezioni di Meccanica Applicata alle Macchine. Edizioni Scientifiche Siderea, 1990.

[20]-Shabana, A.A. Computational Dynamics. John Wiley & Sons, New York, 2001.

[21]-Taniwangsa W., and Kelly, J.M. 1996. Experimental and analytical studies of base isolation applications for low-cost housing. Berkeley, Calif.: Earthquake Engineering Research Center, University of California. UCB/EERC-96/04.

[22]-Tsai, C.S., Lin, Y.C., Su, H.C. Characterization and modeling of multiple friction pendulum system with numerous sliding interfaces. Earthquake Engineering and Structural Dynamics, 2010, 39(13), p. 1463-1491.

[23]-Zayas, V.A., Low, S.S., Mahin, S.A. The FPS earthquake resisting system, Report No. 87-01, Earthquake Engineering Research Center, Berkley, CA, 1987.